# Images of Three Dimensional Flows in Computer Graphics

By

Nobuhide NISHIKAWA,* Akira SUZUKI* and Satoshi AKIYAMA*

(January 27, 1986)

*Summary*: In the present paper the numerical results are shown in graphic images for three dimensional boundary-layer flows. It is shown that the presentation of images especially in solid model graphics allows us to utilize our widest band width sense in an effective manner to create physical or geometrical models and to understand their behavior in simulated environments. As the results, external streamlines and limiting streamlines obtained with finite difference calculations are given for parboloid, and for the front half region of wing-ellipsoid combination.

## §I. INTRODUCTION

Numerical study for three dimensional boundary layer has been appearing within last nearly two decades [*1,2*]. However their illustrations are two dimensional images and do not give 3-D images straightforwardly.

Recently, especially for commercial usage, solid modeler graphics have been developed which allow the definition of complex three dimensional models in a form that the resulting data base can be accessed for a variety of purposes. For example, it has become possible to define very rapidly the geometric boundaries of an vehicle, and then to call for computational grids in numerical computation. A line-printer output is sometimes a heavy load on us in detecting uninvited or expected behaviors of solutions and so on. The presentation of these image allows a person to utilize his widest band width sense, vision, in an effective manner to create models and to understand their behavior in simulated environments. The presentation of this pattern type information is greatly facilitated by the use of computer graphics technique. The incorporation of perspective and the optional removal of hidden lines improved the usefulness of graphic displays. Thus, so called CASD [Computor Aided Software Design] should be introduced in the Computational Fluid Mechanics, while at present a few academic results [*3*] are known in our country.

For the presentation of graphic images or for the data base to the graphics we refer our three dimensional boundary layer solutions [*4,5*]. The pictures by solid model graphics are shown for the external flow field and limiting streamlines for both paraboloid and wing-ellipsoid combination. In the finite difference calculation [*4,5*] the nose coordinates originally devised for body of revolution [*2*] are applied. We show the following examples: first, as for relatively simple case the flow over a paraboloid, and second the flow field on the body of a wing-ellipsoid combination up to the region near the root

* Faculty of Engineering, Chiba University.

location of wing. The finite difference solutions are obtained for 3-D boundary layer with the Box schemes.

The descriptions about the data structure for the computer graphics are given briefly at the end of the present report. The comparison with the images by wire-flame model and the effect of shading on 'solid model images' is also shown. In the last chapter we briefly discuss benefits of 3-D computer graphics.

## §II. Formulation

### 2.1 Basic Equations

For a paraboloid at incidence and in an incompressible laminar flow the governing boundary layer equations can be written in the curvilinear orthogonal coordinate $x$, $\theta$, $y$ as follows

$$\frac{\partial}{\partial x}(h_2 u)+\frac{\partial}{\partial \theta}(h_1 w)+\frac{\partial}{\partial y}(h_1 h_2 v)=0 \tag{1}$$

$$\frac{u}{h_1}\frac{\partial u}{\partial x}+\frac{w}{h_2}\frac{\partial u}{\partial \theta}+v\frac{\partial u}{\partial y}+K_2 w^2=-\frac{1}{\rho h_1}\frac{\partial p}{\partial x}+\nu\frac{\partial^2 u}{\partial y^2} \tag{2}$$

$$\frac{u}{h_1}\frac{\partial w}{\partial x}+\frac{w}{h_2}\frac{\partial w}{\partial \theta}+v\frac{\partial w}{\partial y}+K_2 uw=-\frac{1}{\rho h_2}\frac{\partial p}{\partial \theta}+\nu\frac{\partial^2 w}{\partial y^2} \tag{3}$$

Here $u$, $w$ are the velocity component parallel to the body surface in the meridional and azimuthal directions, respectively, while $v$ is the component normal to the surface, and where $\rho$, $\nu$ are the density and kinematic viscosity, respectively.

Further, $h_1$, $h_2$ are metric coefficients and in this paper the shape of body is chosen such that $h_1$ $h_2$ satisfy the following relations, denoting the nose radius of a body as $R$, and $a$, $b$, are the major-axis-length and radius of equatorial-crosssection of ellipsoid.

$$h_2=2R(x/R)^{1/2}: \quad \text{for parabolid} \tag{4}$$

$$h_2=b(1-(x/a)^2)^{1/2}: \quad \text{for wing-ellipsoid combination} \tag{5}$$

$$h_1=\left(1+\left(\frac{\partial h_2}{\partial x}\right)^2\right)^{1/2} \tag{6}$$

and $K_2$ is the geodesic curvature of surface lines x=constant.

$$K_2=-\frac{1}{h_1 h_2}\frac{\partial h_2}{\partial x} \tag{7}$$

### 2.2 Application of Nose Coordinate

To overcome the difficulty in solving the Eqs. (1)–(3) at the nose the following transformation originally proposed by Stewartson [2] is applied to the paraboloid

$$X=S\cos\theta,\quad Z=S\sin\theta,\quad Y=y/R\,(\mathrm{Re})^{1/2} \tag{8}$$

$$u=U\cos\theta+W\sin\theta,\quad w=W\cos\theta-U\sin\theta,\quad v=V/u_0\,(\mathrm{Re})^{1/2} \tag{9}$$

where $u_0$ is oncoming velocity, and $\mathrm{Re}=v_0\,R/v$.

$$\frac{dS}{S}=\frac{h_1}{h_2}dx \tag{10}$$

The above $X$, $Z$ coordinate system still has disadvantages in the actual calculation, therefore the so called third transformation is introduced in the form of $\tilde{R}$, $\phi$ polar coordinates on curved surface. The origin of the polar coordinate is the stagnation point where $X=X_0$ and the equations for the transformation are as follows.

$$X=X_0+3X_0\tilde{R}(\tilde{R}+\cos\phi)\Delta,\quad Z=3X_0\tilde{R}\Delta\sin\phi;\quad \Delta=1/(1+2\tilde{R}\cos\phi+\tilde{R}^2) \tag{11}$$

$$\left.\begin{aligned} U&=\tilde{R}QD\Delta-\tilde{R}T(1-\tilde{R}^2)\sin\phi\Delta\\ W&=\tilde{R}\Delta\sin\phi[(1-\tilde{R}^2)Q+DT];\quad D=\cos\phi(1+\tilde{R}^2)+2\tilde{R}\end{aligned}\right\} \tag{12}$$

The surface grid lines for $y=0$ given by Eqs. [*11,12*] or nose coordinate are shown in Figs. 1, 2 respectively for the front view and perspective view. In these figures $\phi$=constant lines emanate from the stagnation point and intersect $\tilde{R}$=constant lines, orthogonally.

Thus for the range of $0\leq\tilde{R}\leq0.5$ the integration of equations for $Q$, $T$ and $V$ was proceeded from $\phi=0$ to $\phi=\pi$ along each $\tilde{R}$-constant line. The value of $T$ at the free stream changes its sign in accordance with both the sign and magnitude of $\cos\phi$ for small $\tilde{R}$. Therefore, the Zig-Zag box scheme was employed for all mesh points at $0\leq\tilde{R}\leq0.5$.

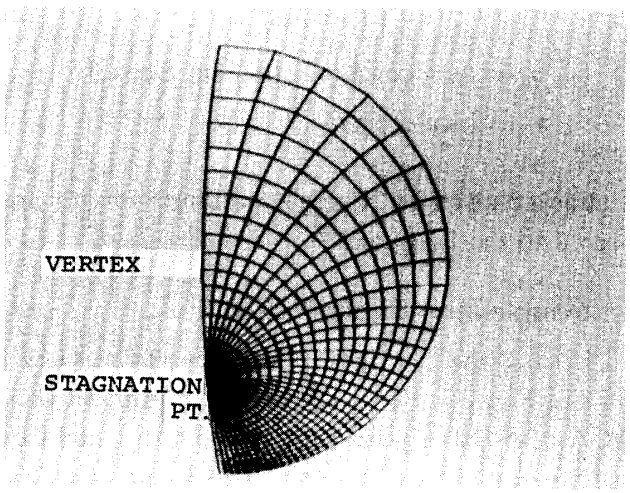


Fig. 1. Nose coordinate for paraboloid: Front view.

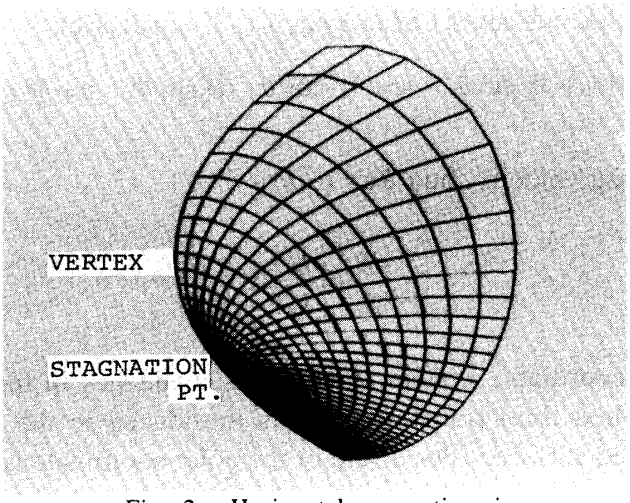


Fig. 2. Horizontal perspective view.

## §III. Boundary Conditions

### 3.1 Calculation at Aft Body

For the aft-body at $x>x_c$ where $X_c=2x_{stag}$ *at* $\tilde{R}=0.5$ we introduce a two component vector potential and boundary layer variable $n=y/(u_e v s_1)^{1/2}$ together with the definition of arclength $s_1$ along a generator.

The boundary conditions become

$$n=0, \quad u=w=v=0, \qquad n=\infty, \quad u/u_e=1, \quad w/w_e=1 \tag{13}$$

### 3.2 External Flow Field: Paraboloid

An inviscid theory gives the velocity components at the boundary layer edge along the paraboloid

$$u_e=\cos\alpha\cos\theta-2\sin\alpha\sin\beta\cos\theta \tag{14}$$

$$w_e=2\sin\alpha\sin\theta \tag{15}$$

where $\alpha$ is angle of attack chosen as 20 deg. and $\tan\beta=\partial h_2/\partial x$ and $\beta$ is the inclination angle of surface referred to the body axis.

### 3.3 External Flow: Wing-ellipsoid combination

The model treated [5] has the configuration whose front view illustrating the panel elements is shown in the Fig. 3. Here, the configuration consists of the body and the non-swept wing(NACA-65A010) whose central and horizontal camber plane tangential to $\theta=45°$ generator of the body at the equator. The body is an axisymmetric ellipsoid at angle of attack 4 deg with axis length ratio 1/5. Thus, the span of the wing corresponds to the region $0>x/a>-0.4$. For this wing-ellipsoid combination the inviscid flow was calculated by Yanagizawa & Kikuchi [6] for the complete body by a Panel-BEM method.

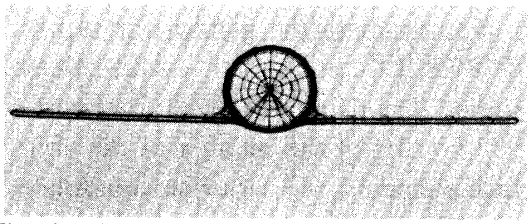

Fig. 3. Front view of wing-ellipsoid combination.

On the generator of body started from the rear end of the wing, a vortex line was assumed to exist. Nine circumferential division was chosen for the inviscid calculation. Therefore for giving smooth boundary-layer-edge condition a third order interpolation was applied to 50 division calculation with boundary layer equation, however a quadratic interpolation was applied along $x$-direction.

As seen in the one of the earliest finite difference solution [*6*] for 3-D boundary layer, a configuration often treated in our field is the flow over the flat plate with circular cylinder normal to the plate. Their results clarified that the earliest separation point appears at $2.5\cdot(R_{\text{cylinder}})$ ahead from the center of the cylinder. Recently, an integral method was applied to a single fuselage-shape by Hirschel [*7*], and the separation near the rear end of body was discussed. In our second example the wing and the curved body surface are respectively corresponding to the cylinder and the flat plate.

## §IV. Numerical Procedures

### 4.1 Numerical Schemes for 3-D Boundary Layer

The numerical program devised by us is the application of the Keller Box scheme. Since principles of our scheme are similar to those by Cebeci *et al* [*2*] as far as in the region without flow-reversal, the description about details of a scheme for a standard 3-D box scheme is omitted here.

The 3-D calculation in this paper consist of the marching along $x$ -direction only on the symmetry lines and marching along $\theta$ -direction. Finite difference equations expressed in terms of variables on neighboring four grid lines are solved in the 3-D version of the bos scheme.

Finite difference equations together with boundary conditions were linearized and iteratively solved by Newton method. The resulting linear system was solved by the LU decomposition. This procedure requires three or four times iteration when the convergence criterion is less than $10^{-5}$. As stated in the above section the Zig-Zag box scheme was applied to the region at $x<x_c$ where the flow is described in terms of nose variables Q and T. The Zig-Zag Box scheme was also applied to the region of reversed circumferential flow ahead or windward side of the estimated separation point. At a separation point the iteration breaks down due to the negative small value of meridional velocity $u$ near the surface.

### 4.2 Procedures for Computer Graphics

We describe the process how the data of the finite difference results are extracted and reordered to compatible to the data structure accessed by our facility for graphics

[GRAPHICA M-1008]. For example the pattern for skinfriction-line or the 'Oil dot pattern' need the data of 380 KB for about 2000 surface elements among which the 'Oil Dot' is expressed as triangle. The data transferred from host computer [HITAC M-180] to be accessed by M-1008 consist of the number of the unit of macroscopic solid, the number of nodes of surface elements, the cartesian coordinates of nodes, the indices for the relation of nodes and so on. In the assist of algebraic function for polygons in the solid model software inconsistencies between coordinate values for nodes induce no visible disorder in images. That is, small overlap as for surfaces due to inconsistency between the location of wing-root and the body surface is recovered automatically and a smooth image can be produced. This is one of large conveniences in the solid modeler tool.

In our faciliy the total number of the commands are about twenty, and parameters for each command are usually not necessary and 5 parameters is demanded exceptionally, e.g. for the location of viewpoint or the colors. The total elapsed time is about one minutes from first command to last one through the manual input from keyboard. After this, repetition of 5 or 6 commands leads to the refining of colors or viewpoint for images.

In this M-1008 we can change the angles of viewpoint referred to the object with input parameters from keyboard, while the size of figures or shift of windows can be varied continuously with the 'roller ball' or the multiplier key on the keyboard. The number of vertices of surface element can be chosen as arbitrary integer less than 9.

## §V. Results and Discussion

Usual curvilinear orthogonal coordinate applied for the surface of the paraboloid is shown in Fig. 4. The defects of line drawings in our solid model software appears here again. The 'Numerical Taft Visualization' or the external velocity vectors are shown in Figs. 5, 6 respectively for side view and bottom view. The automatic shading processing in our graphic facility has a negative contribution to the clearness of picture in the edge region of the body. The monochromatic photograph taken from original color image on the display does not well illustrate the impressive scene on the color display.

The skinfriction vectors obtained by finite difference calculation are shown in the form of 'Oil Dot Pattern' as Fig. 7 for side view. An intersting comparison can be made between the calculated limiting streamline and the photograph of the visualization of

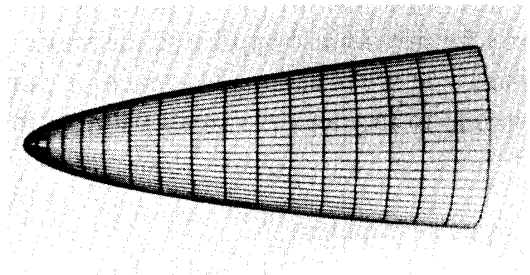

Fig. 4. Surface Grid Lines in usual Curvilinear Coordinate.

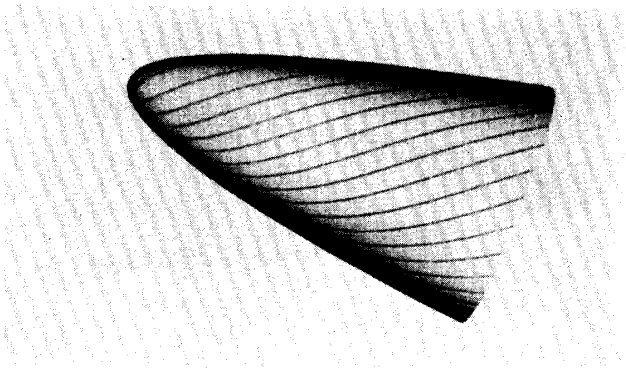

Fig. 5. External Stream line: Side View.

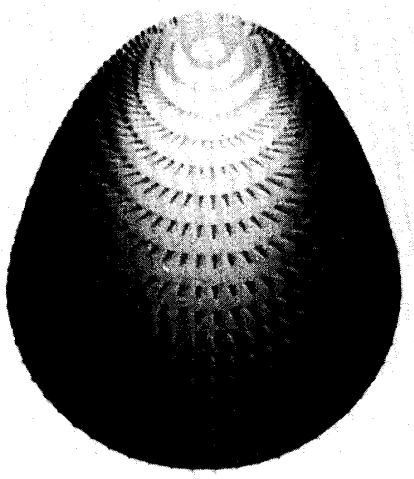

Fig. 6. External Stream velocity vector: bottom view.

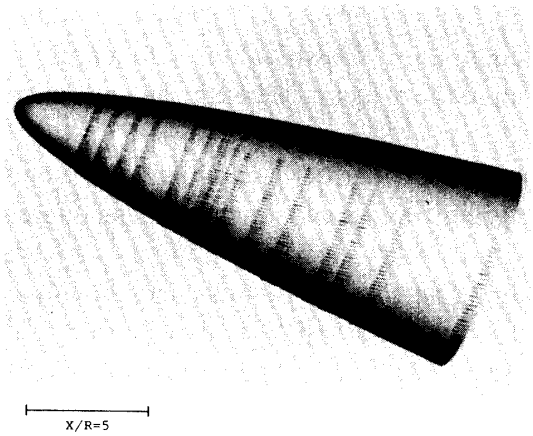


Fig. 7. Skinfriction vectors: Side View, body length $x/R_{\mathrm{nose}}=20$.

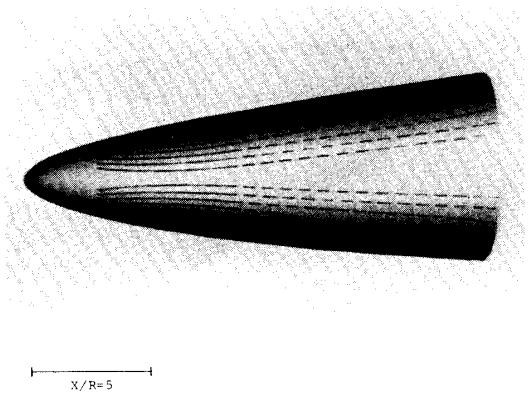


Fig. 8a. Limiting Stream Line: Top View.

Fig. 8b. Flow visualization in Water towing tank. electrolysis method.

streamlines very near the model surface in water towing tank, respectively in Figs. 8a and 8b. The latter visualization was worked out with color up in the electrolysis of salt water with phenolphthalein. The similar flow pattern can be observed in these figures, although the Reynolds number referred to body length is about $5.2\times10^3$.

The comparaison of pictures by wire flame model in Fig. 9a and present 'solid model' is shown in the following figures. 9b, c, d. The incorporation of perspective and the optional removal of hidden lines shown in Fig. 9b improved the usefulness of our facilities. On the other hand the effect of shading can appear in Figs. 9c, d which are the solid model images.

The limiting streamline on the wing-body combination is shown in Fig. 10. The lower four streamlines near the wing-root terminate with the encounter to the separation points. In the present results we designate a separation point as a point at $f''=0.1$ just before the break down of calculation. The computation has been continued so far up to $x=-0.38$ as shown in [5]. The reason is that a rapid increase in the width of the separated region upper the wing is not so plausible to show the validity of boundary layer computation in this region.

In the present case the separation first appears at $X=-0.584$, $\theta=21.6$ deg. The circumferential deviation of start of separation from centerline is about 24 degree, and corresponding distance ahead of the wing leading edge at the root station is 0.059. It is interesting that in this case the circumferential reverse cannot be detected before the break down of calculation or separation. The skinfriction line near the fairing has nearly similar direction of upper surface of wing-root which means that the separation line is

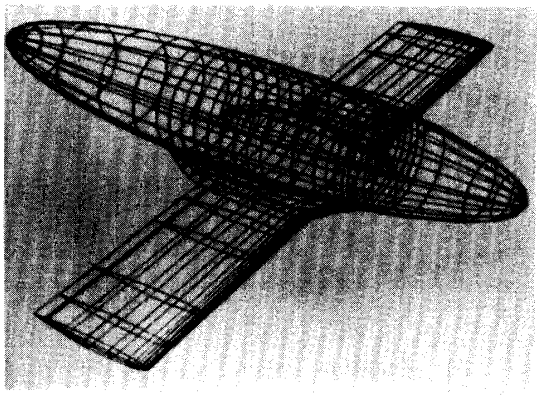

Fig. 9a. Wire flame figure for Wing Body Combination.

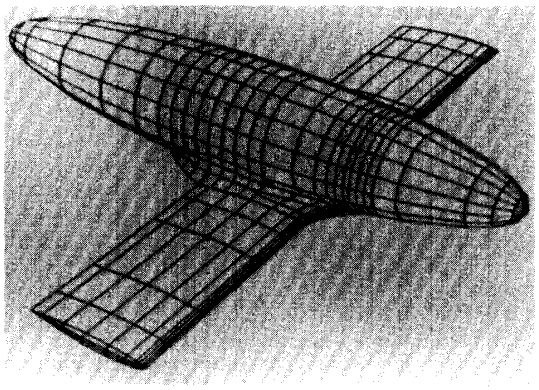

Fig. 9b. Hidden Line Removed.

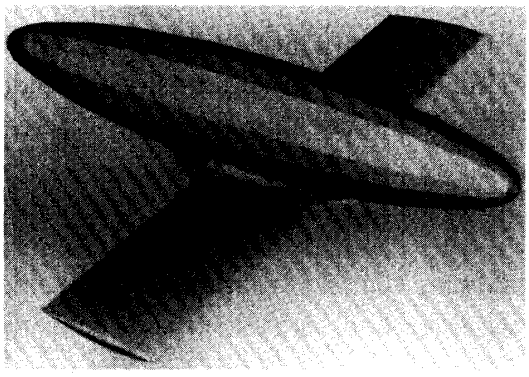

Fig. 9c. Solid Model of Fig 9b.

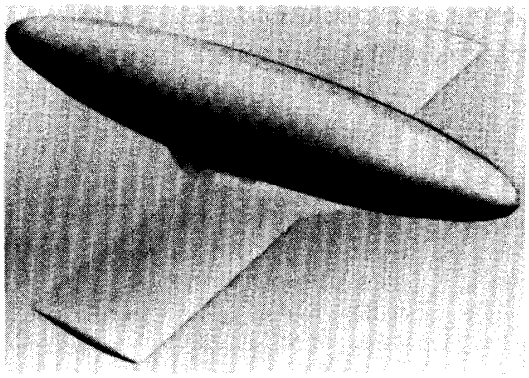

Fig. 9d. Solid Model with Shading.

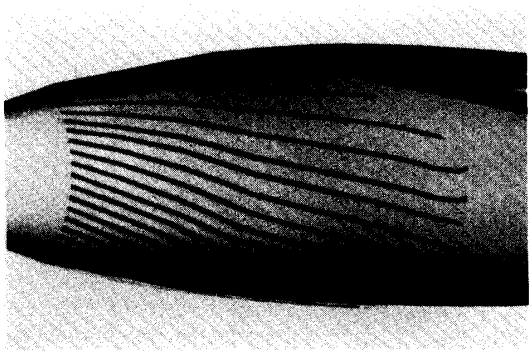

Fig. 10. Limiting Stream Line around Root of Wing.

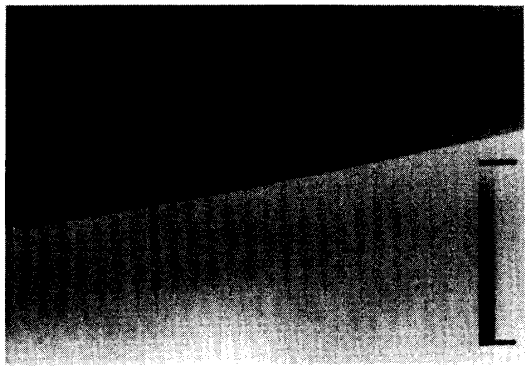

Fig. 11. Pressure distribution on delta wing in incompressible flow.

geometrically similar to the shape of wing in this region.

The pressure distribution obtained with vortex-lattice method [*9,10*] is shown in Fig. 11 for subsonic delta wing with 20 deg dihedral angle at zero incidence angle.

## §VI. Conclusions

We can induce the following remarks from the above examples.

1. The vectors along the three dimensional surfaces are satisfactorily illustrated with the solid model graphics.
2. If the 3-D graphics are easily accessed by a scientist, the process or understanding may reach the deep meaning of the solution.
3. Productivity of development of the computer program or a scheme will be increased.

## References

[ *1* ] Wang, K.C.: Proc. Roy. Soc. A340, pp. 33–55 (1974).
[ *2* ] Cebeci, T. Khattab, A.K., and Stewartson, K., J. Fluid Mech.: *107* (1981) p.57.
[ *3* ] Himeno, R., and Kuwahara, K.: AIAA Paper *85–1617*.
[ *4* ] Nishikawa, N.: Transactions Japan Soc. Aeron. Space Sciences, Vol. 28, No. 79, pp. 27–43 (1985).
[ *5* ] Nishikawa, N.,: Proc. 3rd Symposium of Numerical & Physical Aspects of Aerodynamic Flows pp. 10–35 *10–43* (1985, Jan, Long Beach USA).

[ *6* ] Yanagizawa, M. & Kikuchi, K.: Technical Rep. of National Aerospace Labo., TR-729 (1982, Aug, in Japanese).
[ *7* ] Dwyer, H.A.: Solution of Tree-Dimensional Boundary-Layer flow with Separation, AIAA J. Vol. 6 (1968) pp. 1336–42.
[ *8* ] Hirschel, E.H.: AIAA-Paper *83*–0455.
[ *9* ] Margason, R.J., and Lamar, J.E.: NASA TN D-6 *42* (1971).
[ *10* ] Kobayakawa, M., Onuma, H., Nishida, M., Ohara, A., and Kawakami, Y.: J. Japan Soc. Aeron. and Space Sciences., Vol. 32, No. 363, pp. *232–241* (1984).